



**HAL**  
open science

## Compositional accuracy of atom probe tomography measurements in GaN: Impact of experimental parameters and multiple evaporation events

Enrico Di Russo, Ivan Blum, Jonathan Houard, M. Gilbert, Gérald da Costa, D. Blavette, Lorenzo Rigutti

► **To cite this version:**

Enrico Di Russo, Ivan Blum, Jonathan Houard, M. Gilbert, Gérald da Costa, et al.. Compositional accuracy of atom probe tomography measurements in GaN: Impact of experimental parameters and multiple evaporation events. *Ultramicroscopy*, 2018, 187, pp.126–134. 10.1016/j.ultramic.2018.02.001 . hal-01928843

**HAL Id: hal-01928843**

**<https://hal.science/hal-01928843v1>**

Submitted on 20 Jul 2020

**HAL** is a multi-disciplinary open access archive for the deposit and dissemination of scientific research documents, whether they are published or not. The documents may come from teaching and research institutions in France or abroad, or from public or private research centers.

L'archive ouverte pluridisciplinaire **HAL**, est destinée au dépôt et à la diffusion de documents scientifiques de niveau recherche, publiés ou non, émanant des établissements d'enseignement et de recherche français ou étrangers, des laboratoires publics ou privés.

# Compositional accuracy of atom probe tomography measurements in GaN: Impact of experimental parameters and multiple evaporation events

E. Di Russo, I. Blum, J. Houard, M. Gilbert, G. Da Costa, D. Blavette, L. Rigutti\*

UNIROUEN, INSA Rouen, CNRS, Groupe de Physique des Matériaux, Normandie Université, 76000 Rouen, France

## ABSTRACT

A systematic study of the biases occurring in the measurement of the composition of GaN by Atom Probe Tomography was carried out, in which the role of surface electric field and laser pulse intensity has been investigated. Our data confirm that the electric field is the main factor influencing the measured composition, which exhibits a deficiency of N at low field and a deficiency of Ga at high field. The deficiency of Ga at high field is interpreted in terms of preferential evaporation of Ga. The detailed analysis of multiple evaporation events reveals that the measured composition is not affected by pile-up phenomena occurring in detection system. The analysis of correlation histograms yields the signature of the production of neutral  $N_2$  due to the dissociation of  $GaN_3^{2+}$  ions. However, the amount of  $N_2$  neutral molecules that can be detected cannot account for the N deficiency found at low field. Therefore, we propose that further mechanisms of neutral N evaporation could be represented by dissociation reactions such as  $GaN^+ \rightarrow Ga^+ + N$  and  $GaN^{2+} \rightarrow Ga^{2+} + N$ .

### Keywords:

Atom probe  
GaN  
Composition analysis  
Metrology  
Compositional accuracy

## 1. Introduction

Laser-assisted Atom Probe Tomography (La-APT) is currently applied to the investigation of both structure and composition of semiconductors. However, compositional measurements are often strongly affected by compositional biases. This clearly emerges from several studies in which the composition of some oxides (ZnO, MgO), nitrides (GaN, AlN) and ternary alloys (MgZnO, AlGaIn) was investigated [1–4].

In this work we systematically study compositional biases occurring in the atom probe analysis of GaN, in order to gain a better understanding about the physical phenomena that are involved in such biases. In particular we investigated the experimental conditions leading to deviations from the expected Ga/N ratio equal to 1, which corresponds to its stoichiometric composition.

We have investigated the role of laser pulse energy, surface electric field and detection rate on compositional measurements. Our results show that the surface electric field is the only physical parameter that acts on composition measurements. At high surface field, Ga deficiency is observed, which can be explained by Ga preferential evaporation (i.e. evaporation not synchronized with the laser pulse). At low field however, N deficiency is observed. As

it has been suggested, this could be caused by emission of neutral N-based molecules that cannot be detected in atom probe experiments [5,6].

Finally, recent observations indicate that the formation of molecular ions and their field dissociation can affect composition measurements [5,7]. The mechanisms that promote both formation and dissociation of molecular ions are not well understood: experiments show at least that non-dissociated group-V molecular ions are more abundant at low field conditions [1,8]. Furthermore, theory shows that dissociation can be promoted by the high electric field surrounding the tip and/or by the fact that molecules can leave the tip in an excited state [9,10]. Moreover, dissociation processes and correlated evaporation can lead to intrinsic detection issues (pile-up effect), which reduce the probability of detecting certain ions [8,11]. In this article, a quantitative analysis of multiple events allows us to determine the impact of these phenomena on the accuracy of composition measurements in atom probe tomography, and to suggest an alternative mechanism of N loss that should be ascertained with theoretical means.

## 2. Experimental

In order to perform Laser-assisted Atom Probe Tomography (La-APT), [0001] oriented GaN specimens were prepared by standard Scanning Electron Microscope/Focused Ion Beam (SEM/FIB) annular milling with 30kV Ga ions and cleanup procedure with Ga ions

\* Corresponding author.

E-mail address: [lorenzo.rigutti@univ-rouen.fr](mailto:lorenzo.rigutti@univ-rouen.fr) (L. Rigutti).

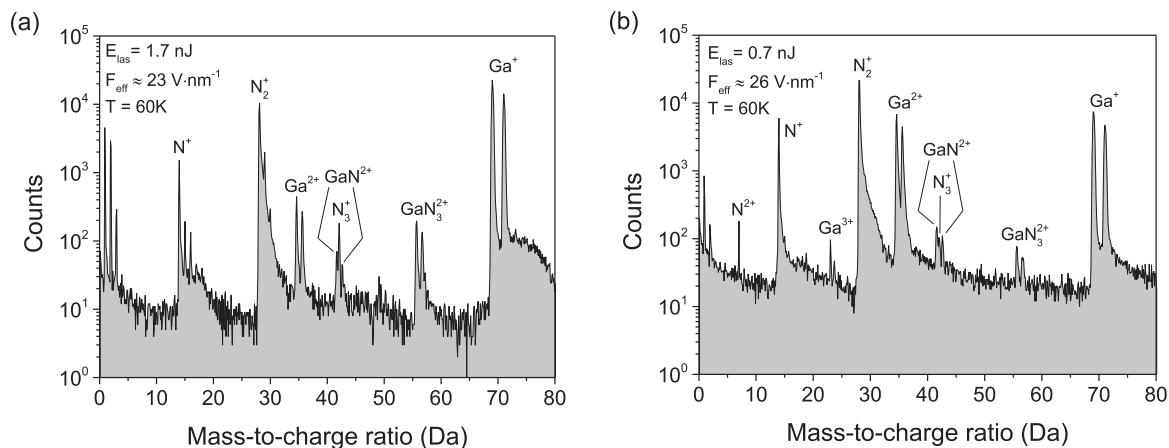


**Fig. 1.** GaN mass spectra measured at constant detection rate using: (a) laser pulse energy  $E_{las} = 1.7$  nJ (UV), effective field  $F_{eff} \approx 23$  V nm $^{-1}$ ; (b)  $E_{las} = 0.7$  nJ (UV),  $F_{eff} \approx 26$  V nm $^{-1}$ . The number of ions detected for each dataset is close to  $2.1 \times 10^5$ . The specimen base temperature was  $T = 60$  K and the detection rate  $\varphi \approx 0.0025$  event/pulse. Experiments were performed using FlexTAP.

at 2 kV [12,13]. In this way, needle-shaped atom probe specimens with  $\sim 50$  nm radius at the apex and a cone angle of equal to  $2.5^\circ$  were obtained.

Analyses were performed using two different tomographic atom probes, LaWaTAP and FlexTAP, operated with femto-second laser pulses (350 fs) focused to a  $20 \mu\text{m}$  diameter spot [14]. Measurements were performed using a laser wavelength  $\lambda = 343$  nm (UV). The laser repetition frequency was 100 kHz in LaWaTAP and 50 kHz in FlexTAP.

During measurements the laser pulse energy  $E_{las}$  ranged between 0.1 and 40 nJ. The corresponding peak intensities are reported in Supplementary Material. The specimen base temperature  $T$  was set to different values ranging from 30 to 60 K.

In both instruments the detection system used was a specially designed multi-channel plate/advanced delay line detector (MCP/aDLD) with a MCP efficiency  $\eta_{MCP} \approx 0.6$  [15,16]. The field of view of the LaWaTAP is fixed at  $\pm 18^\circ$ . The FlexTAP uses electrostatic lenses to modulate the trajectories of the ions and allows measurements at different fields of view (from  $\pm 8^\circ$  up to  $\pm 30^\circ$ ) [16]. For this study, the field of view was set to  $\pm 18^\circ$  in order to match the one of the LaWaTAP atom probe.

The role of the experimental parameters on the measured composition was investigated performing three different series of measurements: i) at constant detection rate  $\varphi$ , varying both applied bias  $V_{DC}$  and laser energy  $E_{las}$ ; ii) at constant laser pulse energy  $E_{las}$ , with the applied bias  $V_{DC}$  varying; iii) at constant applied bias  $V_{DC}$ , with the laser pulse energy  $E_{las}$  varying.

Finally, Field Ion Microscopy (FIM) experiments were performed within the LaWaTAP instrument using a mixture of He/Ne in proportions (2/3) at a pressure of  $2 \times 10^{-5}$  mbar.

### 3. Results and discussion

#### 3.1. GaN mass spectra

Two experiments were first performed using the FlexTAP instrument. Laser energies of 0.7 and 1.7 nJ were used while the tip voltage was varied so as to maintain the detection rate  $\varphi$  close to 0.0025 event/pulse in both cases. The specimen base temperature was set to 60 K and the number of ions detected for each dataset was  $2.1 \times 10^5$ .

The two corresponding mass spectra, Fig. 1-(a and b) exhibit common features. The peak at 14 Da can be attributed to  $N_2^{2+}$ ,  $N^+$  or a mixture of both. In principle, the presence of  $N_2^{2+}$  can cause an additional peak at 14.5 Da, corresponding to  $(^{14}\text{N}^{15}\text{N})^{2+}$

molecules, which should not appear in the presence of  $N^+$  ions only. However, the  $^{15}\text{N}$  natural abundance is equal to 0.36% only. Thus, even if all nitrogen was ionized as  $N_2^{2+}$ , the peak at 14.5 Da should still correspond to only 0.7% of all those events, which would still be below the background noise in the present mass spectra. Thus, our experimental results do not give information about the presence or absence of  $N_2^{2+}$  ions. Theoretical considerations can be helpful in this case. The double ionization of  $N_2$  molecules is reported to take place at  $60$  V nm $^{-1}$  [5]. However, GaN evaporates at a much lower field, about  $23 \div 26$  V nm $^{-1}$ , as suggested by previous studies conducted by Mancini et al. and Agrawal et al. [1,17]. Therefore, we considered that the double ionization of  $N_2$  is unlikely in our experiment and assume that the peak at 14 Da is entirely associated to  $N^+$ . In any case the choice between  $N_2^{2+}$  and  $N^+$  does not change considerably the measured composition, as most nitrogen is detected as  $N_2^+$ , which can be unambiguously attributed. The high number of  $N_2^+$   $N_2^+$  ions suggests the presence of short range diffusion and/or surface reconstruction phenomena. N-N bonds are indeed not present in GaN structure and during the field evaporation of the tip, small  $\text{Ga}_n\text{N}_m$  ( $n, m > 1$ ) clusters can be formed on its surface. The simulations performed by Song et al. show that N-rich clusters have a larger binding energy than Ga-rich clusters [18]. Moreover, it is shown that  $\text{Ga}_n\text{N}_m$  structures are dominated by  $N_2$  or  $N_3$  subunits and can dissociate into smaller clusters.  $N_2$  molecules can be produced in this way. Similar results were obtained by Costales et al. who studied the evolution of chemical bonding of III-nitrides clusters [19]. These simulations are supported by atom probe measurements in which  $N_2^+$ ,  $N_3^+$ ,  $\text{GaN}^{2+}$  and  $\text{GaN}_3^{2+}$  molecular ions are detected [1]. No peaks at 97 and 99 Da, corresponding to  $\text{GaN}_2^+$  molecular ions, were observed.

It should be noted that  $N_3^+$ ,  $\text{GaN}^{2+}$  and  $\text{GaN}_3^{2+}$  molecular ions are more abundant at high  $E_{las}$  conditions, which correspond to a low  $V_{DC}$  applied, as can be observed in Fig. 1. Other differences can be identified. A few peaks are visible only at low laser power: two small peaks around 23 Da which were identified as  $\text{Ga}^{3+}$  and one peak at 7 Da, which was identified as  $N_2^+$ , which is consistent with the fact that higher charge states are expected to be more abundant at higher electric fields. Also, when using low  $E_{las}$  and high  $V_{DC}$  the GaN spectrum is affected by a larger background noise, which is related to DC field evaporation. The signal to noise ratio is  $1.2 \cdot 10^2$  at  $E_{las} = 1.7$  nJ and decreases to  $0.5 \cdot 10^2$  at  $E_{las} = 0.7$ . Conversely, high  $E_{las}$  leads to more pronounced thermal tails in the spectrum. This clearly suggests lower heat dissipation for increasing laser energy. As the UV laser spot has a diameter of about

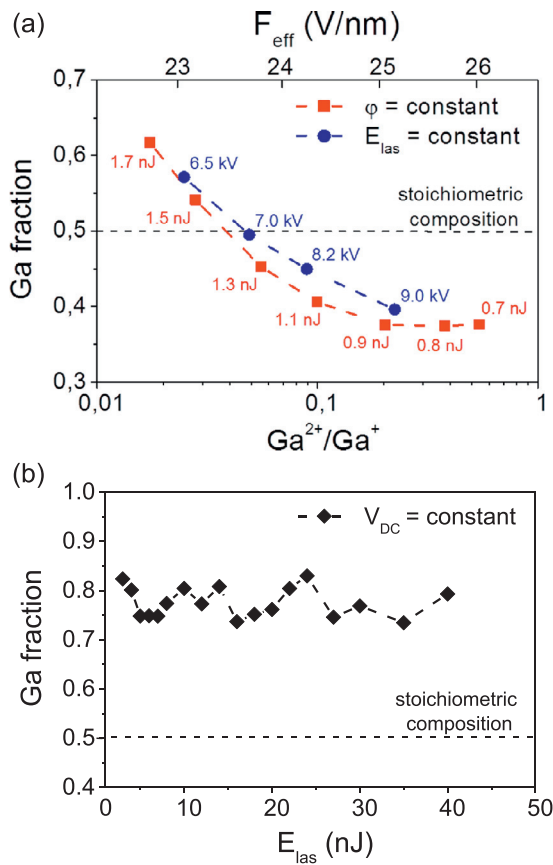


**Fig. 2.** (a) Ga fraction plotted as a function of  $Ga^{2+}/Ga^+$  ratio for: (■) constant detection rate  $\varphi \approx 0.0025$  event/pulse; (●) constant laser pulse energy  $E_{las} = 5$  nJ (UV). Specimen base temperature  $T = 60$  K. (b) Ga fraction plotted as a function of laser pulse energy  $E_{las}$ .  $V_{DC} = 6.5$  kV,  $T = 50$  K. The measurements at constant detection rate and constant  $V_{DC}$  field were performed using FlexTAP, while the measurements at constant laser pulse energy were performed using LaWaTAP.

20  $\mu\text{m}$ , these tails are also generated from the heated parts of the specimen at a distance of few  $\mu\text{m}$  from the apex. For this reason, these tails do not present an exponential form. Similar behaviors were recently reported in GaAs atom probe measurements [8]. Parasitic species such as hydrogen-, carbon-, nitrogen- and oxygen-related peaks and hydrides were also detected, most likely supplied by the environment during the specimen preparation procedure. As depicted in Fig. 1-(a and b), these parasitic species are more abundant at low DC field conditions and decrease significantly at high DC field conditions, where only  $H^+$  and  $H_2^+$  ions were detected at 1 and 2 Da respectively. These are general features which have been systematically observed also for other materials. Atom probe mass spectra are known to be strongly affected by the electric field conditions at which measurements were carried out [1,8]. The so-called effective electric field  $F_{eff}$  can be calculated through the Kingham's post-ionization model [20]. To do so, for each experiment, the Ga Charge-State-Ratio (Ga-CSR)  $Ga^{2+}/Ga^+$  was estimated:  $F_{eff}$  was  $\approx 26$  V  $\text{nm}^{-1}$  for the experiment performed at  $E_{las} = 0.7$  nJ and 26 V  $\text{nm}^{-1}$  for the experiment performed at  $E_{las} = 1.7$  nJ.

### 3.2. Influence of experimental parameters on measured composition

The Ga fraction is plotted as a function of the Ga-CSR in Fig. 2-(a) for both experiments discussed in the previous section and experiments performed with intermediate laser energies. The measured Ga fraction varies from 0.6 at  $F_{eff} \approx 23$  V  $\text{nm}^{-1}$  ( $E_{las} = 1.7$ ) to 0.4 at  $F_{eff} \approx 26$  V  $\text{nm}^{-1}$  ( $E_{las} = 0.7$ ). This behavior is qualitatively

similar to what has been found in other III-V semiconductors such as AlN and GaAs [1,8].

It should be reminded that in constant detection rate mode both the surface DC field and the laser energy are varied. Hence it is not possible to discriminate between the influence of the electric field and laser energy on the measured composition with these experiments only. Therefore, we also performed a series of measurements at constant laser energy  $E_{las} = 5$  nJ, with  $V_{DC}$  ranging between 6.5 and 9.0 kV ( $T = 60$  K), and thus, varying detection rate. The instrument used was the LaWaTAP. The results are also reported in Fig. 2-(a).

Both series of experiments yield similar results as a function of the Ga-CSR, as it is shown in Fig. 2-(a). This suggests that the composition depends mainly on  $F_{eff}$ , confirming the general trend reported by different authors [1,8,17,21]. This corroborates the idea that  $E_{las}$  is not a pertinent parameter to compare atom probe measurements all the more that the energy actually transmitted to the tip depends on focusing conditions and on experimental details of the instrument that is used. Moreover,  $E_{las}$  cannot be directly linked to the energy absorbed by the tip, as it depends on the laser wavelength, the tip geometry and the size of the laser spot [11,22]. On the other hand, the Ga-CSR is confirmed to be a reliable parameter for comparing measurements performed with different instruments, such as here with the FlexTAP and LaWaTAP, which are shown to provide results consistent with each other [1,5,17].

Last, a series of measurements was performed at constant applied bias  $V_{DC}$  using the FlexTAP.  $E_{las}$  was varied from 3 to 40 nJ, with  $V_{DC} = 6.5$  kV. The specimen base temperature was 50 K. Due to the small shank angle of the tips, the tip curvature radius was not significantly increased during the measurement. As  $V_{DC}$  remained constant, the measured Ga-CSR also remained approximately constant at  $(5 \pm 1) \cdot 10^{-3}$ , which corresponds to  $F_{eff} \approx 22$  V  $\text{nm}^{-1}$ . This is also a strong indication that the measured Ga-CSR does not depend on  $E_{las}$ . The evolution of the measured composition as a function of  $E_{las}$  is reported in Fig. 2-(b), where each point corresponds to a dataset of  $10^5$  ions detected. Despite the fact that a wide range of laser pulse energies was investigated, the average Ga fraction remains relatively constant. This confirms the hypothesis that the composition depends solely on the surface electric field. Similar behaviors were observed in GaAs where it was shown that the measured Ga-fraction is not significantly affected by  $E_{las}$  [8]. In this case, the Ga fraction remains close to  $0.76 \pm 0.03$  which is larger than the expected stoichiometry (0.5). Clearly, nitrogen is partly lost at low field. Measurements performed at constant applied bias  $V_{DC}$  confirm the general trend observed in Fig. 2-(a).

In the performed set of measurements, no significant differences are found between measurements performed at different specimen base temperatures.

### 3.3. Microscopic field distribution and measurement of composition

The microscopic effect of the electric field on the measured composition was investigated using both APT measurements and FIM. The last was performed using as imaging gas a mix of He (2/5) and Ne (3/5): this combinations provided the best imaging conditions. The specimen base temperature was  $T = 60$  K, and the applied bias was  $V_{DC} = 8$  kV. FIM indeed provides an image of the electric field distribution at the tip surface, as FIM contrast depends on the local electric field. In Fig. 3-(a) we report a FIM micrograph revealing the presence of a central pole identified as the [0001] pole. This pole is a high field region. 6 facets related to the hexagonal wurtzite symmetry can be identified [1,6,16,23,24]. The steady state shape of the tip should be thus six-fold lobed rather than hemispherical due to evaporation field anisotropies. We interpret this as related to different chemical bond strengths along different crystallographic directions.

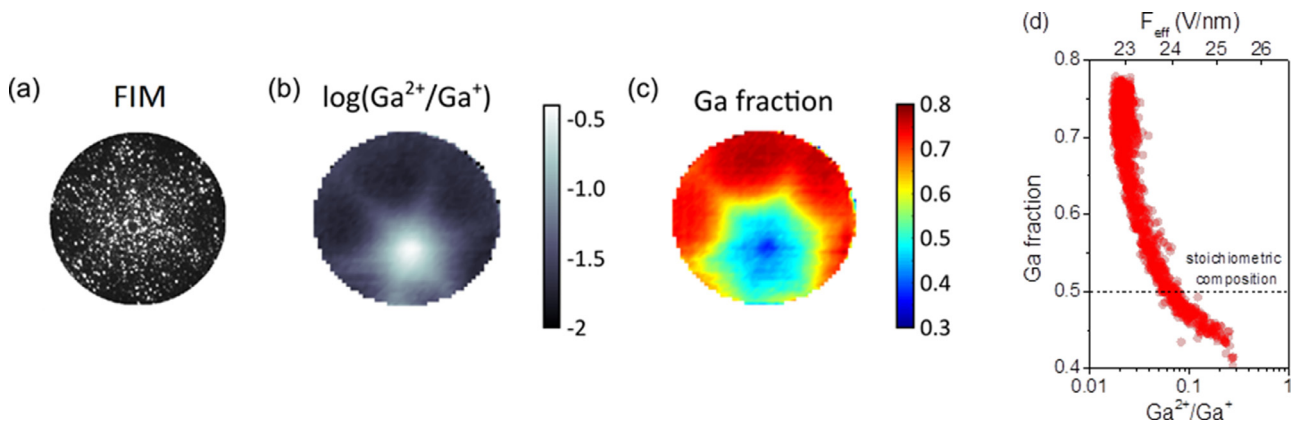


**Fig. 3.** (a) FIM micrograph of GaN surface taken using a mix of He (2/5) and Ne (3/5).  $T=60$  K;  $V_{DC}=8$  kV; FIM gas pressure  $=2 \times 10^{-5}$  mbar. Statistics in the detector space for GaN atom probe tomography: (b) Ga-CSR; (c) Ga fraction at  $\varphi \approx 0.0025$  event/pulse,  $E_{las}=2.1$  nJ,  $T=30$  K. (d) Surface composition distribution of the Ga-fraction as a function of the local Ga-CSR.

In order to correlate FIM and La-APT analysis, a dataset of  $\approx 34$  million events was acquired using the LaWaTAP at constant detection rate using the following parameters:  $T=30$  K;  $E_{las}=2.1$  nJ;  $\varphi \approx 0.0025$  event/pulse. The average distribution of Ga-CSR and Ga-fraction on the tip surface is depicted in Fig. 3. The image is generated adopting the same method described by Mancini et al. in ref. [1]. The detector surface is divided into an array of square pixels. For each of these pixels the number of counted ions allows to locally measure both the Ga-CSR and the detected composition in a space which is a projection of the tip surface. In Fig. 3-(b), the Ga-CSR chart reveals the same field distribution as the FIM micrograph in Fig. 3-(a). Both the [0001] axis pole and the six crystal facets are associated to high field regions. The same pattern appears in the Ga-fraction chart represented in Fig. 3-(c). Again, low Ga fractions are observed in high field regions, suggesting that preferential evaporation of Ga is responsible for this underestimation of the Ga fraction. The six low field facets, on the contrary, are associated with a N-poor composition. A stoichiometric composition was detected only in a thin annular region around the [0001] axis pole, where the field is intermediate. This is in excellent agreement with data presented in Fig. 2-(a). Whatever the analysis parameter used, the stoichiometric composition is never measured over the entire tip surface, even if the average measured composition is equal to the stoichiometric one.

The Ga-fraction at the tip surface as a function of the local Ga-CSR is plotted in Fig. 3-(d). Despite atom probe data correspond to different crystallographic regions on the tip, they are aligned on a single curve with relatively little dispersion. This shows again that the surface electric field is the only relevant physical parameter to explain changes in composition. For low  $F_{eff}$ , a N depletion is measured, while a Ga-depletion is associated with higher  $F_{eff}$  values. Similar behaviors were reported for other III-V semiconductors, such as AlN [1], or ternary compounds such as  $Al_xGa_{1-x}N$  alloy [3]. Moreover, in a recent article, Di Russo et al. studied compositional biases in GaAs [8]. The results also indicate that the measured composition depends on the local field. Essentially, high field conditions lead to a III-group poor measured composition. Instead, low field conditions are associated to a V-group poor measured composition. In order to interpret these common features observed in III-V semiconductors, the hypothesis of preferential evaporation of III-group atoms (i.e. Ga) at high electric field conditions was proposed [1,3,8,21]. On the other hand, the production of neutral V-group molecules (i.e.  $N_2$ ) is suggested to lead to the V-group depletion at low field [5]. La-APT measurements in which the average measured composition corresponds to the stoichiometric one

do not imply that no atoms are lost due to the effects just discussed. In fact, the preferential evaporation of metallic atoms can balance the loss of V-group atoms due to the production of neutral molecules. These considerations strongly suggest that the detection efficiency can be significantly less than  $\eta_{MCP} \approx 0.6$  even if the correct composition is measured. It should be underlined that the measurement of a correct stoichiometry in GaN also depends on the region over which this measurement is defined. An average correct stoichiometry on the whole detector space is the result of higher N loss in low field regions and of higher Ga loss in high field regions. The user should thus keep in mind that the experimental parameters yielding a globally correct stoichiometry are not necessarily the most adapted to the measurement. In the case of a related system, it was proven in the past that it is not possible to obtain all correct atomic fractions in  $Al_yGa_{1-y}N$ , while a correct site fraction  $y$  can be achieved at low field [3]. In the case of GaN, it will be crucial to ascertain under which conditions a correct measurement of the concentration of dopant impurities can be achieved. To the best of our knowledge, such conditions still have to be determined.

#### 3.4. Dependence of multiple-ion events on the experimental parameters

Multiple-ion events correspond to the detection of two or more ions after the same pulse. They can be caused by correlated evaporation, as extensively discussed by Da Costa et al. [16] and De Geuser et al. [25]. Multiple-ion events can give information about possible causes of composition biases. First, they yield information about possible dissociation of molecular ions [8,26], that can lead to the formation of neutral atoms [5]. Secondly, multiple impacts on the detector can cause the pile-up effect, which is a loss of detection efficiency of certain species which occurs when impacts on the detector are too close in time and space to be resolved [8,16].

The distribution of multiple-ion events in constant detection rate mode is reported in Fig. 4-(a) for different electric fields (i.e. different laser energies). It should be noted that the fraction of multiple events of order  $n=1,2,3,\dots$  corresponds here to the fraction of events corresponding to the detection of  $n$  ions evaporated on the same laser pulse, and should not be confused with the fraction of ions detected within multiple events of order  $n$ . At constant evaporation rate, an increase of  $F_{eff}$ , which corresponds to a decrease of  $E_{las}$ , leads to a progressive rise of the fraction of multiple events from 2.9 to 8.8%. This could be caused by an increase in correlated evaporation or dissociation of molecular ions [8,25,26]. In Fig. 4-(b), we report the distributions of detection distances  $d$

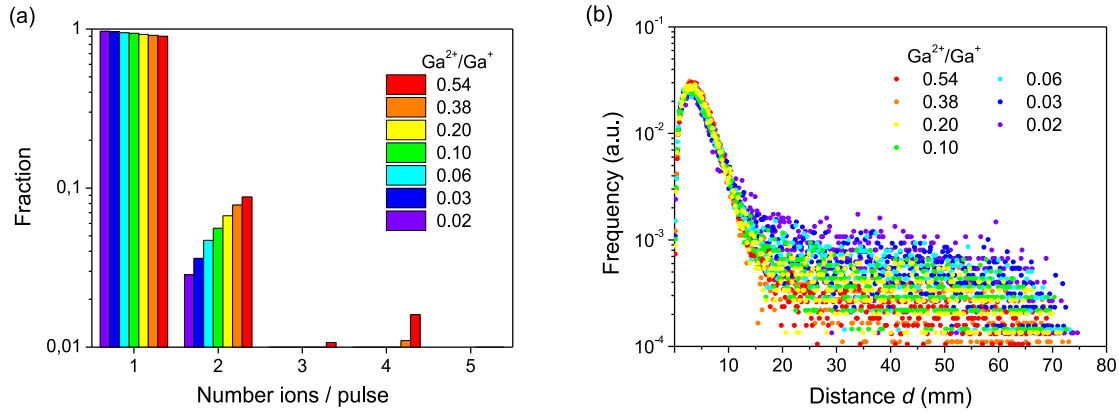


**Fig. 4.** Analysis of multiple-ion events for measurements performed at constant detection rate. (a) Histogram of the fraction of multiple events at different  $E_{las}$ . (b) Histograms of distances between impacts associated with multiple-ion events at different  $E_{las}$ .

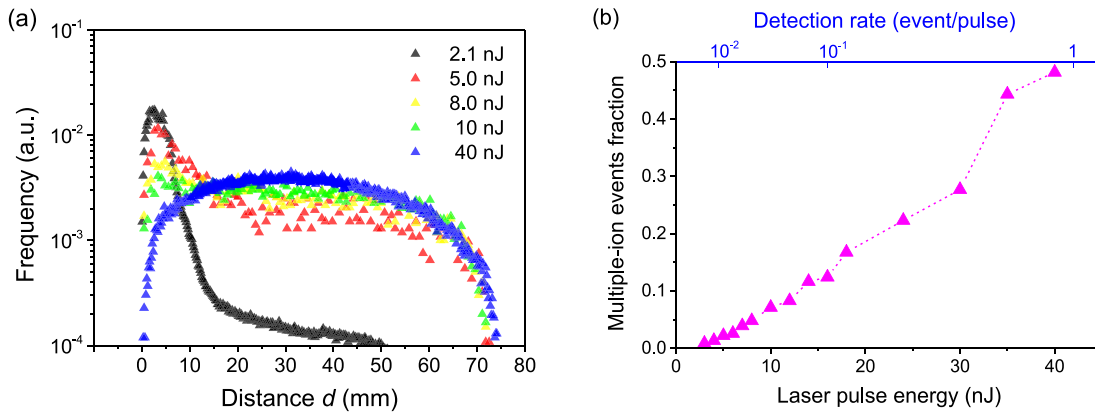


**Fig. 5.** (a) Histograms of distances between impacts associated with multiple-ion events for constant  $V_{DC}$  measurements. (b) Evolution of the fraction of multiple events as a function of  $E_{las}$  in constant  $V_{DC}$  measurements. In the graph is also reported the detection rate at which measurements were carried out.

between ion hits within multiple events at different field conditions. A common behavior is observed whatever the laser energy (i.e. whatever the field): the distribution of impact distances on the detector is bimodal with two contributions. We observe a peak at small distances close to 3 mm, corresponding to spatially correlated events, and a broader distribution weakly decreasing towards larger distances. The amplitude of this second distribution appears to weakly increase at low field conditions. It should be noted that these distributions are the convolution of different distributions associated to at least correlated evaporation, molecules dissociation and un-correlated multiple evaporation events [8,9,25,27]. The shape of these distance distributions does not change as a function of the DC field. Very similar behaviors were found in GaAs as discussed in ref. [8]. In this reference, in particular, the analysis of spatially correlated multi-ions events reveals that the impact of pile-up on the global composition is negligible throughout the whole interval of surface electric field explored.

The role of the laser energy in the generation of multiple-ion events has been investigated at constant fields ( $V_{DC}=6.5$  kV, at  $T=50$  K), with  $E_{las}$  ranging between 2.1 and 40 nJ. As illustrated in Fig. 5-(a), larger  $E_{las}$  leads to a broad distribution with no peak at small distance (3 mm). This indicates that at high  $E_{las}$  multiple-ion events are principally associated with spatially distant and uncorrelated sites at the tip surface.

In measurements performed at constant DC voltage, the increase of  $E_{las}$  leads to an increase of both the detection rate and the fraction of multiple-ion events, as shown in Fig. 5-(b). Nevertheless, as shown in Fig. 2-(b) the measured composition is insensitive to this type of variations.

### 3.5. Identification of molecular dissociation channels

Multiple events related to dissociated molecular ions are of great interest [7,9,26]. These can be studied using correlation histograms [26]. Nevertheless, this approach does not provide information about dissociation processes that take place very close to the tip surface, which cannot be distinguished from spatially correlated multiple-ion events.

As recently investigated by Zanuttini et al. through a theoretical study of the dissociation of  $ZnO^{2+}$  molecules in different dissociation channels containing charged and neutral species, dissociation can have an important role in atom probe measurements [28]. The dissociation of  $ZnO^{2+}$  molecules can occur through different channels, one of which would form neutral O, and would explain the oxygen-poor composition found at low  $F_{eff}$  in ZnO [1,4,28]. Moreover, as shown in ref. [28], such dissociations would take place too close to the specimen surface (at a distance a few ångströms from the tip) to be detected in the correlation histograms.

Similar considerations can be extended to III-V semiconductors where part of the V-group atoms (i.e. nitrogen) can be lost due to production of neutral molecules resulting from dissociation processes [1,5,8,27].

The large dataset that we acquired at constant detection rate was considered in order to analyze the dissociation processes occurring in GaN. The analysis of correlation histogram reported in Fig. 6 allows assessing that part of  $GaN^{2+,3+}$  and  $GaN_3^{2+}$  molecular ions dissociate during their flight. Dissociation is due to the break of a Ga-N bond, that is thought to be weaker than the N-N

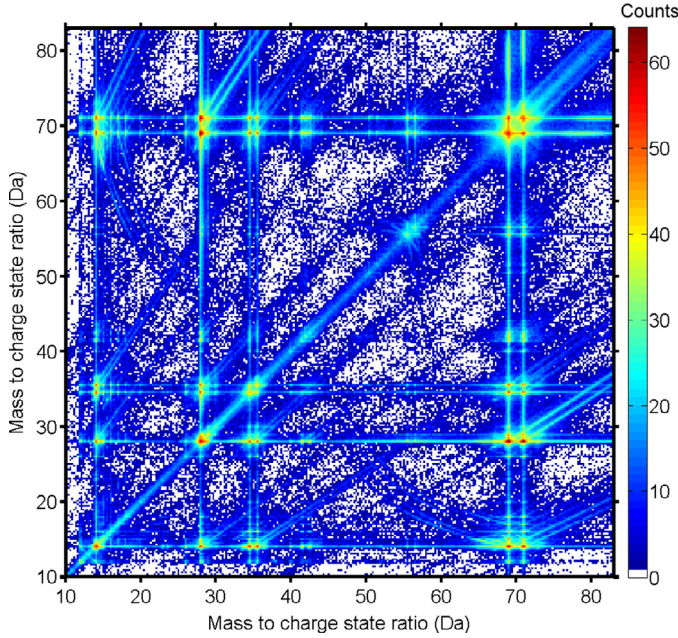


**Fig. 6.** Correlation histogram for the field dissociation of GaN. Analysis parameters:  $\varphi \approx 0.0025$  events/pulse;  $E_{\text{las}} = 2.1$  nJ; average Ga-CSR = 0.045 ( $F_{\text{eff}} \approx 23.5$  V nm $^{-1}$ );  $T = 30$  K.

bond, as demonstrated theoretically by Song et al. [18]. The principal dissociation processes, as reported in ref. [26], are:



Gault et al. recently showed that  $\text{GaN}_3^{2+}$  molecules have a second dissociation pathway leading to the production of neutral  $\text{N}_2$  molecules [5]:



This reaction was proposed to be one of the contributions that lead to selective loss of nitrogen atoms in atom probe experiments [5].

A quantitative analysis of dissociation processes can also be carried out. Firstly, the total amount of neutral  $\text{N}_2$  molecules that are lost due to the dissociation process (4) was determined from the correlation histogram reported in Fig. 6. The very weak dissociation track associated to the process (4) is indicated by the arrow in Fig 7-(a). Taking into account a detection efficiency of 0.6, it was estimated that a maximum of  $4.2 \cdot 10^3$  molecules of  $\text{N}_2$  were emitted. However, as the number of  $\text{N}_2^+$  ions is about  $5.4 \cdot 10^6$ , this very small amount of molecules has almost no influence on the final Ga-fraction measured. Therefore, the dissociation channel (4) cannot apparently be responsible for the N poor composition measured at low  $F_{\text{eff}}$  conditions.

Secondly, the dissociation channel (1) was analyzed in more detail. This one is found to be the most frequent dissociation process observed in GaN. All the ion pairs  $\{\text{}^{69}\text{Ga}^+, \text{}^{14}\text{N}^+\}^{\text{diss.}}$  resulting from dissociation were selected in the correlation histogram and represented inside the box in Fig. 7-(a). Ion pairs were selected if their experimental mass-to-charge ratios were within 0.1 Da from the expected ones for dissociation channel (1). These values can be calculated as reported in ref. [26]. Because in correlation histograms,

dissociation tracks are overlapped with peaks associated to correlated evaporation processes, the  $\{\text{}^{69}\text{Ga}^+, \text{}^{14}\text{N}^+\}^{\text{corr. evap.}}$  ion pairs with a fractional potential drop  $(V_d/V_0) > 0.985$  were not taken into account in dissociation calculations.  $V_0$  here is the DC voltage applied to the tip during this event and  $V_d$  is the potential at which a dissociation event takes place.  $V_d$  can be calculated from measured times-of-flight of the two fragments [7,9,26,28]. In Fig. 7-(b) we have reported the histogram of the fractional potential drop  $(V_d/V_0)$  at which the selected dissociation events occur (i.e.  $(V_d/V_0) = 1$  at the position of the specimen surface;  $(V_d/V_0) = 0$  at the position of the detector). Data show that most dissociation events occur for  $(V_d/V_0) > 0.85$  and a few events are detected for  $0.65 < (V_d/V_0) < 0.85$ . In Fig. 7-(c) we report the distribution of impact distances  $d$  on the detector for the  $\{\text{}^{69}\text{Ga}^+, \text{}^{14}\text{N}^+\}^{\text{diss.}}$  ion pairs resulting from the dissociation of  $\text{GaN}^{2+}$  molecules. It shows a broad peak at 5.4 mm, which is larger than the  $\sim 3$  mm average distance that is measured when considering all multiple events. This large distance between impacts is most probably caused by coulomb repulsion between dissociation products [9,27]. In order to verify this, the impact distances  $d$  on the detector of  $\{\text{}^{69}\text{Ga}^+, \text{}^{14}\text{N}^+\}^{\text{diss.}}$  couples resulting from dissociation of  $\text{GaN}^{2+}$  were simulated for different dissociation angles  $\alpha_d$ . This angle is defined as the orientation of the  $\text{GaN}^{2+}$  molecule axis with respect to the electric field upon dissociation. At  $\alpha_d = 0^\circ$  the N is toward the detector, while  $\alpha_d = 180^\circ$  corresponds to the Ga toward the detector [9,10]. The simulation has taken into account the conditions at which experimental data were collected: the tip geometry, the electric field conditions around the tip and the configuration of the analysis chamber. The dissociation energy was set equal to 8 eV. This value was calculated from simulations of field-induced molecular dissociation of GaN molecules, adopting the same approach described in ref. [28]. The results of these simulations are reported in Fig. 7-(d). The simulated trajectories reveal that for  $(V_d/V_0) > 0.85$ ,  $d$  is ranging between 1 and 10 nm and depends on both  $\alpha_d$  and  $V_d/V_0$ . Despite the simulations being rather qualitative, it is interesting to compare these with experimental data. This comparison suggests that a broad experimental distribution is compatible with the dissociation of  $\text{GaN}^{2+}$  molecules at different dissociation angles  $\alpha_d$  at  $(V_d/V_0) > 0.85$ . Contrariwise, the distance distribution of  $\{\text{}^{69}\text{Ga}^+, \text{}^{14}\text{N}^+\}^{\text{corr. evap.}}$  pairs presents a peak at 1.9 mm. A similar value is found for other ion pairs associated to correlated evaporation phenomena, i.e.  $\{\text{}^{69}\text{Ga}^+, \text{}^{71}\text{Ga}^+\}$  ion pairs. It should be noted that hetero-isotopic Ga couples were chosen instead of the homo-isotopic ones in order to avoid the pile-up phenomenon which sets a limit to the ion pair detection at low distance  $d$ . These results strongly suggest that the ions pair  $\{\text{}^{69}\text{Ga}^+, \text{}^{14}\text{N}^+\}^{\text{corr. evap.}}$  are associated to correlated evaporation processes and no dissociation events were detected for  $(V_d/V_0) > 0.985$ . The probability per second that the dissociation process  $(\text{}^{69}\text{Ga}^{14}\text{N})^{2+} \rightarrow \{\text{}^{69}\text{Ga}^+, \text{}^{14}\text{N}^+\}$  occurs as a function of the lifetime is reported in Supplementary Material.

Finally, the fraction of  $(\text{}^{69}\text{Ga}^{14}\text{N})^{2+}$  molecules which dissociates in  $\{\text{}^{69}\text{Ga}^+, \text{}^{14}\text{N}^+\}$  ion pairs was calculated. The real number of  $(\text{}^{69}\text{Ga}^{14}\text{N})^{2+}$  molecules  $N_{\text{mol}}$  ( $\frac{M}{m} = 41.5$  Da) that reach the detector and that do not dissociate was derived from the number of detected events  $N_{\text{peak}}$  at 41.5 Da and the detector efficiency  $\eta_{\text{MCP}}$ :

$$N_{\text{mol}} = \frac{N_{\text{peak}}}{\eta_{\text{MCP}}}. \quad (5)$$

The number of  $(\text{}^{69}\text{Ga}^{14}\text{N})^{2+}$  molecules  $N_{\text{mol}}^*$  that reach the detector after the dissociation into  $\{\text{}^{69}\text{Ga}^+, \text{}^{14}\text{N}^+\}$  ion pairs  $N_{\text{pairs}}$  is:

$$N_{\text{mol}}^* = \frac{N_{\text{pairs}}}{\eta_{\text{MCP}}^2}. \quad (6)$$

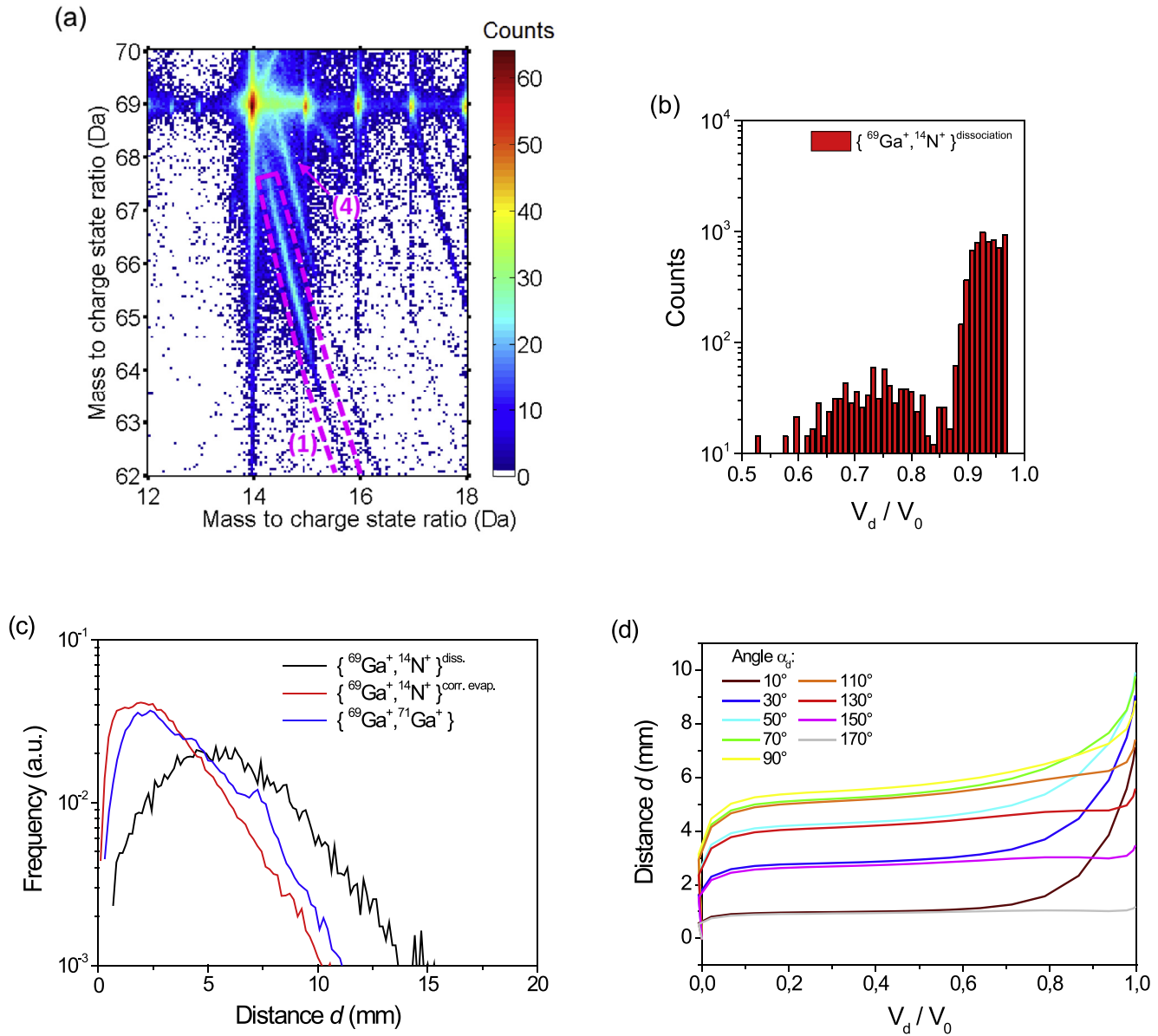


**Fig. 7.** (a) Detail of the correlation histogram of GaN reported in Fig. 6. The ion pairs  $\{^{69}\text{Ga}^+, ^{14}\text{N}^+\}^{\text{diss.}}$  resulting from the dissociation process (1) are represented inside the box. The weak dissociation track associated with process (4) is indicated by the arrow. (b) Histogram of the relative potential drop ( $V_d/V_0$ ) at which the events associated to the dissociation process inside the box in Fig. 7-(a) occurs. (c) Histograms of distances between impacts associated with multiple-ion events associated to the  $\{^{69}\text{Ga}^+, ^{14}\text{N}^+\}^{\text{diss.}}$ ,  $\{^{69}\text{Ga}^+, ^{14}\text{N}^+\}^{\text{corr. evap.}}$  and  $\{^{69}\text{Ga}^+, ^{71}\text{Ga}^+\}$  ion pairs. (d) Simulation of the impact distances  $d$  as a function of the fractional potential drop ( $V_d/V_0$ ) and the dissociation angle  $\alpha_d$  for dissociation process (1).

The fraction  $f$  of  $(^{69}\text{Ga}^{14}\text{N})^{2+}$  molecules that dissociate is provided by the following equation:

$$f = \frac{N_{\text{mol}}^*}{N_{\text{mol}}^* + N_{\text{mol}}} = \frac{N_{\text{pairs}}}{N_{\text{pairs}} + \eta_{\text{MCP}} \cdot N_{\text{peak}}}. \quad (7)$$

In Eq. (7) it should be noted that  $f$  depends on the detection efficiency  $\eta_{\text{MCP}}$  which was set to 0.6. The fraction  $f$  is estimated to be  $\approx 0.3 \div 0.4$  throughout the  $F_{\text{eff}}$  range investigated.

The correlation between ion pairs involved in multiple ion events was studied adopting the method of the correlation tables described by Saxey [26]. This method consists of comparing the number  $p_{ij}$  of each ion-pair  $ij$  with the expected number of coincidences  $e_{ij}$  calculated under the hypothesis of independent co-evaporation, so that  $e_{ij} = e_i \times e_j$ , where  $e_i$  is the fraction of the  $i$ -th species in the multiple-event mass spectrum. Both  $p_{ij}$  and  $e_{ij}$  are  $n \times n$  matrices ( $n$  being the number of considered species). The de-

gree of correlation between measured and expected number of ion pairs is given by the following matrix:

$$c_{ij} = \frac{p_{ij} - e_{ij}}{e_{ij}}, \quad (8)$$

where  $c_{ij}$  represents the degree of correlation (when  $c_{ij} > 0$ ) or anti-correlation (when  $c_{ij} < 0$ ) between ion pairs. Due to pile-up effects, the measured degree of correlation is lower than the real one:  $p_{ij} (\text{measured}) < p_{ij} (\text{real})$ . In order to correct this effect, the diagonal values  $c_{ii}$  are artificially set equal to zero. Moreover, similarly to what is made in chi-squared tests, low  $p_{ij}$  entries ( $< 5$ ) are considered as not statistically significant. Fig. 8-(a) depicts the correlation table associated to an effective field  $F_{\text{eff}} \approx 23 \text{ V nm}^{-1}$ , while the correlation table in Fig. 8-(b) is associated to  $F_{\text{eff}} \approx 25 \text{ V nm}^{-1}$ . The number of ion pairs for each ion  $i$  is also given. For both the values of  $F_{\text{eff}}$  investi-

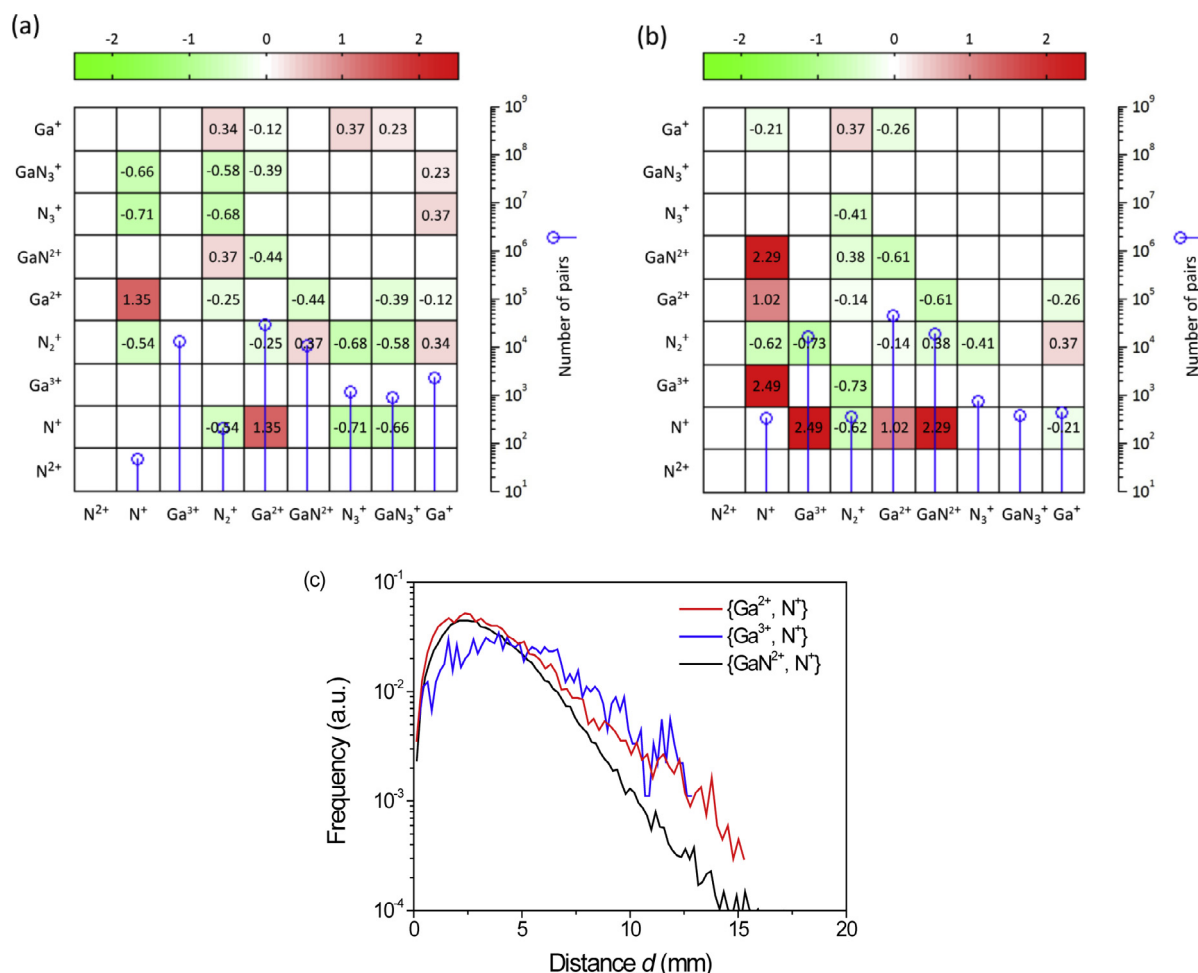


**Fig. 8.** Correlation tables associated with different field conditions: (a)  $F_{eff} \approx 23 \text{ V nm}^{-1}$ ; (b)  $F_{eff} \approx 25 \text{ V nm}^{-1}$ . In the tables also the number of ion pairs associated to each species are reported. Data are referred to the following experimental parameters:  $T = 30 \text{ K}$ ;  $\varphi \approx 0.0025 \text{ event/pulse}$ ;  $E_{las} = 2.1 \text{ nJ}$ . (c) Distribution of impact distances  $d$  associated to some selected ion pairs.

gated  $\{Ga^{2+}, N^+\}$  ion pairs appear strongly correlated. Instead,  $\{Ga^{3+}, N^+\}$  and  $\{GaN^{2+}, N^+\}$  ion pairs appear correlated only for  $F_{eff} \approx 25 \text{ V nm}^{-1}$ . It should be noted that during the tip evaporation the local field at terrace edges can be temporarily and locally larger than  $25 \text{ V nm}^{-1}$ . The value of  $F_{eff}$  that is given here is an average over time. This can justify the production of triple ionized Ga ions observed at  $F_{eff} \approx 25 \text{ V nm}^{-1}$ , when the theory of post ionization predicts this charge state to appear at a field of  $35 \text{ V nm}^{-1}$  [20]. Ion pairs which exhibit high correlation can result from either molecule dissociation or correlated evaporation phenomena [8,26,27]. In order to distinguish these processes, the distribution of impact distances  $d$  associated to the three ion pairs was considered (Fig. 8-(c)). Data show that both  $\{Ga^{2+}, N^+\}$  and  $\{GaN^{2+}, N^+\}$  ion pairs present a distance distribution very similar to those reported in Fig. 7-(a) for correlated evaporation events, with a peak at  $d \approx 2.3 \text{ mm}$ . This strongly suggests that these ion pairs are mostly associated with correlated evaporation processes. Instead,  $\{Ga^{3+}, N^+\}$  ion pair exhibits a slightly broader and shifted (larger  $d$ ) distribution. However this distance distribution is fairly similar to those reported in Fig. 7-(a) for correlated evaporation processes. Thus, there is no striking evidence to suggest that  $\{Ga^{3+}, N^+\}$  ion pairs are associated to some dissociation processes.

In conclusion, no clear experimental evidence of dissociation processes close to the tip surface emerges from our analysis. The only dissociation reactions producing at least two charged fragments are those identified in the correlation histogram. However,

besides the reaction (4) producing too few molecules to account for the observed N loss, it still remains possible that dissociation reactions producing one charged and one neutral fragment take place, similarly to the case of the  $ZnO^{2+} \rightarrow Zn^{2+} + O$  reaction in ZnO [28]. This reaction produces indeed a neutral fragment that is not detected at low field, and that becomes post-ionized at higher field, consistently with the experimental behavior of ZnO during the APT analysis [28]. In the case of GaN, the reactions  $GaN^{2+} \rightarrow Ga^{2+} + N$  and  $GaN^+ \rightarrow Ga^+ + N$  represent the most interesting candidates for a theoretical study. It must be underlined, in fact, that differently to the case of dissociation reactions producing neutral fragments in  $SiO_x$  [10], these specific reactions would not leave a trace in atom probe data, and their possible occurrence should be investigated with dedicated theoretical tools.

#### 4. Conclusions

In summary, we have carried out a thorough investigation of the dependence of the measured GaN composition over experimental conditions. Our results confirm that the main driving parameter for the occurrence of compositional biases is the surface electric field. The composition is observed to be Ga-rich (i.e. N-depleted) at low field, Ga-poor (i.e. N-rich) at high field. This can be explained by an increase of Ga preferential evaporation at high field, and by neutral N emission at low field. Several mechanisms of neutral N production were proposed. We carried out a thor-

ough analysis of the multiple events, in order to elucidate whether neutral N emission could be evidenced, and if this can explain the observed composition biases. It is shown that multiple detection events have no significant effect on the measured composition in GaN. The origin of compositional biases in atom probe measurements of GaN is not determined by intrinsic detection issues which can be put in evidence through the analysis of multiple hits. The analysis of correlation histograms indicate the signature of neutral production, but the amount of neutrals that can be inferred from them is too small to account for the observed bias at low field. It was also shown that in correlation histograms only a part of the dissociation processes can be revealed: dissociation processes close to the tip surface cannot be revealed adopting this approach. In order to verify if dissociation also takes place very close to the tip surface, correlation tables for various electric fields were examined. The analysis of the charts reveals that some ion pairs exhibit strong correlation. However, the study of the impact distances of these pairs on the detector shows that these are principally associated to correlated evaporation processes. In conclusion, no dissociation processes producing charged fragments close to the tip surface were evidenced. However, dissociation processes producing one charged ion and one neutral N could take place and would not be detected. Dedicated theoretical approaches are needed to investigate this issue.

#### Acknowledgment

This work was funded by the [French National Research Agency \(ANR\)](#) in the framework of the projects EMC3 Labex AQRATE and ANR-13-JS10-0001-01 TAPOTER.

#### Supplementary materials

Supplementary material associated with this article can be found, in the online version, at [doi:10.1016/j.ultramic.2018.02.001](https://doi.org/10.1016/j.ultramic.2018.02.001).

#### References

- [1] L. Mancini, N. Amirifar, D. Shinde, I. Blum, M. Gilbert, A. Vella, F. Vurpillot, W. Lefebvre, R. Lardé, E. Talbot, P. Pareige, X. Portier, A. Ziani, C. Davesne, C. Durand, J. Eymery, R. Butte, J.-F. Carlin, N. Grandjean, L. Rigutti, *J. Phys. Chem. C* 118 (2014) 24136.
- [2] E. Di Russo, L. Mancini, F. Moyon, S. Moldovan, J. Houard, F.H. Julien, M. Tcherycheva, J.M. Chauveau, M. Hugues, G. Da Costa, I. Blum, W. Lefebvre, D. Blavette, L. Rigutti, *Appl. Phys. Lett.* 111 (2017) 032108.
- [3] L. Rigutti, L. Mancini, D. Hernandez-Maldonado, W. Lefebvre, E. Giraud, R. Butte, J.F. Carlin, N. Grandjean, D. Blavette, F. Vurpillot, *J. Appl. Phys.* 119 (2016) 105704.
- [4] N. Amirifar, R. Lardé, E. Talbot, P. Pareige, L. Rigutti, L. Mancini, J. Houard, C. Castro, V. Sallet, E. Zehani, S. Hassani, C. Sartel, A. Ziani, X. Portier, *J. Appl. Phys.* 118 (2015) 215703.
- [5] B. Gault, D.W. Saxe, M.V. Ashton, S.B. Sinnott, A.N. Chiramonti, M.P. Moody, D.K. Schreiber, *New J. Phys.* 18 (2016) 033031.
- [6] D.R. Diercks, B.P. Gorman, R. Kirchhofer, N. Sanford, K. Bertness, M. Brubaker, *J. Appl. Phys.* 114 (2013) 184903.
- [7] D. Santhanagopalan, D.K. Schreiber, D.E. Perea, R.L. Martens, Y. Janssen, P. Khalifah, Y.S. Meng, *Ultramicroscopy* 148 (2015) 57.
- [8] E. Di Russo, I. Blum, J. Houard, G. Da Costa, D. Blavette, L. Rigutti, Field-dependent measurement of GaAs composition by atom probe tomography, *Microsc. Microanal.* 23 (6) (2017) 1067–1075.
- [9] I. Blum, L. Rigutti, F. Vurpillot, A. Vella, A. Gaillard, B. Deconihout, *J. Phys. Chem. A* 120 (20) (2016) 3654.
- [10] D. Zanuttini, I. Blum, L. Rigutti, F. Vurpillot, J. Douady, E. Jacquet, P.-M. Anglade, B. Gervais, *J. Chem. Phys.* 147 (2017) 164301.
- [11] M. Müller, G.D.W. Smith, B. Gault, C.R.M. Grovenor, *J. Appl. Phys.* 111 (2012) 064908.
- [12] S. Padalkar, J.R. Riley, Q. Li, G.T. Wang, L.J. Lauhon, *Phys Status Solidi C* 11 (3–4) (2014) 656.
- [13] I. Blum, F. Cuvilly, W. Lefebvre-Ulrikson, Chapter four—atom probe sample preparation, in: *Atom Probe Tomography*, Academic Press, 2016, pp. 97–121.
- [14] L. Arnoldi, E.P. Silaeva, A. Gaillard, F. Vurpillot, I. Blum, L. Rigutti, B. Deconihout, A. Vella, *Am. J. Appl. Phys.* 115 (2014) 203705.
- [15] G. Da Costa, F. Vurpillot, A. Bostel, B. Deconihout, *Rev. Sci. Instrum.* 76 (2005) 013304.
- [16] G. Da Costa, H. Wang, S. Duguay, A. Bostel, D. Blavette, B. Deconihout, *Rev. Sci. Instrum.* 83 (2012) 123709.
- [17] R. Agrawal, R.A. Bernal, D. Isheim, H.D. Espinosa, *J. Phys. Chem. C* 115 (2011) 17688.
- [18] B. Song, P.-L. Cao, *Phys. Lett. A* 328 (2004) 364.
- [19] A. Costales, M.A. Blanco, Á.M. Pendás, A.K. Kandalam, R. Pandey, *J. Chem. Am. Soc.* 124 (2002) 4116.
- [20] D.R. Kingham, *Surf. Sci.* 116 (1982) 273.
- [21] J. Riley, R.A. Bernal, Q. Li, H. D.Espinosa, G.T. Wang, L.J. Lauhon, *ACS Nano* 6 (5) (2012) 3898.
- [22] A. Vella, *Ultramicroscopy* 132 (2013) 5.
- [23] F. Tang, M.P. Moody, T.L. Martin, P.A. Bagot, M.J. Kappers, R.A. Oliver, *Microsc. Microanal.* 21 (2015) 544.
- [24] B. Bonef, R. Cramer, J.S. Speck, *J. Appl. Phys.* 121 (2017) 225701.
- [25] F. De Geuser, B. Gault, A. Bostel, F. Vurpillot, *Surf. Sci.* 601 (2007) 536.
- [26] D.W. Saxe, *Ultramicroscopy* 111 (2011) 473.
- [27] M. Müller, D.W. Saxe, G.D.W. Smith, B. Gault, *Ultramicroscopy* 111 (2011) 487.
- [28] D. Zanuttini, I. Blum, L. Rigutti, F. Vurpillot, J. Douady, E. Jacquet, P.-M. Anglade, B. Gervais, *Phys. Rev. A* 95 (6) (2017) 061401.